Ultrasonics Sonochemistry 34 (2017) 774–780

Contents lists available at ScienceDirect

Ultrasonics Sonochemistry

journal homepage: www.elsevier.com/locate/ultson

Fe-based heterogeneous catalysts for the Fischer-Tropsch reaction: Sonochemical synthesis and bench-scale experimental tests

Alberto Comazzi [a,*], Carlo Pirola [a], Mariangela Longhi [a], Claudia L.M. Bianchi [a], Kenneth S. Suslick [b]

[a] Università degli Studi di Milano, Dipartimento di Chimica, via Golgi, 19, 20133 Milano, Italy
[b] University of Illinois at Urbana-Champaign, School of Chemical Sciences, 505 S. Mathews Av., Urbana, IL 61801, USA

ARTICLE INFO

Article history:
Received 3 May 2016
Received in revised form 12 July 2016
Accepted 19 July 2016
Available online 19 July 2016

Keywords:
Fischer Tropsch
Iron based catalysts
Ultrasound
Syngas
Sonochemical synthesis

ABSTRACT

The sonochemical synthesis of nanostructured materials owes its origins to the extreme conditions created during acoustic cavitation, *i.e.*, the formation of localized hot spots in the core of collapsing bubbles in a liquid irradiated with high intensity ultrasound (US). In particular, in the present work a sonochemical synthesis has been investigated for the production of three different iron-based samples supported on SiO_2 and loaded with different metals and promoters (10 %wt of Fe; 30 %wt of Fe; 30 %wt of Fe, 2 % wt of K and 3.75 %wt of Cu) active in the Fischer-Tropsch (FT) process. Sonochemically synthesized heterogeneous catalysts were characterized by BET, XRPD, TPR, ICP, CHN, TEM, SEM and then tested in a fixed bed FT-bench-scale rig fed with a mixture of H_2 and CO at a H_2/CO molar ratio equal to 2, at activation temperatures of 350–400 °C and reaction temperatures of 250–260 °C. The experimental results showed that the ultrasonic samples are effective catalysts for the FT process. Notably, increasing the activation temperature increased CO conversion, while product selectivity did not diminish. All the sonochemically prepared samples presented in this work provided better catalytic results compared to the corresponding traditional FT impregnated catalysts.

1. Introduction

The chemical consequences of the ultrasonic irradiation of liquids has been a topic of substantial research over the past several decades [1–7]. The power of ultrasound (US) originates from the physical phenomena of the acoustic cavitation, *i.e.*, the formation, growth and implosion of bubbles in a liquid. The implosive collapse of the bubbles generates extreme conditions in which very high temperatures ($T \approx 5000$ K), cooling rates (10^9 °C/s) and pressures ($P \approx 150$ MPa) are locally reached [8]. These particular conditions can be used in several ways for a wide variety of chemical reactions, extraction processes, and the production of nanostructured materials.

Nanostructured materials find diverse applications in the development of magnetic devices, photoelectronic devices such as semiconductors, and heterogeneous catalysts. These materials have different chemical-physical properties compared to traditional bulk materials, and can be synthesized with different preparation methods such as gas-phase techniques (*e.g.*, pyrolytic decomposition of volatile organometallic compounds), liquid-phase methods (*e.g.*, reduction of metal halides), and mixed-phase approaches (*e.g.*, metal atom vapor deposition into cryogenic liquids).

As reported in the literature, the use of US has already been tested in the production of several nanostructured materials and devices [9]. One possible US-assisted method for the synthesis of heterogeneous catalysts uses traditional preparation methods such as impregnation with ultrasound in order to optimize the dispersion of the inorganic precursors on the support surface [10]. Another approach involves the sonochemical decomposition of volatile organometallic precursors like metal carbonyls dispersed in high boiling solvents in the presence of an inorganic support (*e.g.*, SiO_2, Al_2O_3 or TiO_2) where the exposure of carbonyls like Fe $(CO)_5$ and/or $Co_2(CO)_8$ to ultrasound produces amorphous metallic (M^0) nanoparticles on the support surface [11].

In addition to the power, frequency, and duration of the ultrasound, the vapor pressure of both reactants and solvent are crucial parameters for the preparation of these kinds of materials. The volatility of the precursors is key because the sonochemical reaction begins within the vapor of the collapsing bubble. In addition, the vapor pressure of the solvent should be low (*i.e.*, high boiling point); otherwise, the presence of high concentrations of solvent vapor in the collapsing bubble will reduce the efficiency of the collapse process. This synthetic method offers a way to produce metal-based catalysts with more uniform size distribution, higher

* Corresponding author.
E-mail address: alberto.comazzi@unimi.it (A. Comazzi).

http://dx.doi.org/10.1016/j.ultsonch.2016.07.012
1350-4177/

surface area and a more controlled phase composition than the catalysts synthesized with traditional techniques (*e.g.*, incipient wetting with metal salts) [11].

One challenging application of heterogeneous catalysis is in the Fischer-Tropsch (FT) process (*i.e.*, reduction and oligomerization of CO with H_2). The FT synthesis is a highly exothermic ($\Delta_r H \approx -200\ kJ \cdot mol^{-1}$) oligomerization reaction in gas phase which produces hydrocarbons, *e.g.*, fuels and waxes, and some oxygenated compounds, in the range of C_1-C_{100} using syngas, *i.e.* a mixture of H_2 and CO with an H_2/CO ratio equal to 2 [12,13]. The typical FT process requires iron or cobalt based catalysts. Cobalt is more active and has a greater selectivity towards linear, high molecular weight products while iron is less expensive and active for the Water Gas Shift (WGS) reaction making it a suitable FT catalyst even if syngas with H_2/CO ratio lower than 2 (*i.e.* synthesis gas produced from biomass called bio-syngas [14,15]) is fed into the reactor. In addition, supported iron-based catalysts have several advantages (*e.g.*, greater surface area, better dispersion of heat generated by the reaction and better mechanical resistance) in comparison to the massive iron catalysts adopted in current FT industrial plants [16]. The main reactions of the FT process are given in the following Eqs. ((1)–(5)):

Alkanes production:

$$(2n+1)\ H_2 + n\ CO \rightarrow C_nH_{2n+2} + n\ H_2O \quad (1)$$

Alkenes production:

$$2n\ H_2 + n\ CO \rightarrow C_nH_{2n} + n\ H_2O \quad (2)$$

Production of oxygenated compounds:

$$2n\ H_2 + n\ CO \rightarrow C_nH_{2n+2}O + (n-1)\ H_2O \quad (3)$$

Boudouard reaction:

$$2\ CO \leftrightarrow CO_2 + C \quad (4)$$

WGS synthesis (with iron-based catalysts):

$$H_2O + CO \leftrightarrow H_2 + CO_2 \quad (5)$$

SiO_2 supported iron based catalysts synthesized with traditional impregnation methods have been compared with the use of US in several works by Suslick et al. [8,11] and Pirola et al. [10]. In the former, the synthesis of an iron-based sample with 10%wt of active metal was achieved with the US decomposition of $Fe(CO)_5$ where the catalyst was tested at different temperatures and low pressure (100 kPa) without oxidizing the Fe^0 present on the SiO_2 surface before the FT runs. In the second case, a different series of iron-based samples with different loadings of iron and promoters were synthesized by sonicating an aqueous solution containing the dissolved inorganic precursors and then tested at high pressure (2.0 MPa) and various temperatures.

This work presents the sonochemical synthesis of three different iron-based samples on a SiO_2 support with different amount of Fe and promoters (10 %wt of Fe; 30 %wt of Fe; 30 %wt of Fe, 2 %wt of K and 3.75 %wt of Cu) exploiting the US decomposition of $Fe(CO)_5$ and a simpler way to oxidize these catalysts over prior proposed synthesis methods. The optimized loadings of Fe and promoters were determined in a previous work by Pirola et al. [17]. The presence of the promoters plays an important role in the catalytic process, potassium in particular improves CO adsorption on the catalyst surface [18] and copper promotes the reduction of the iron oxide phase from hematite (Fe_2O_3) to magnetite (Fe_3O_4) then further to iron metal or iron carbide, the active species for the FT reaction [19].

The samples have been characterized by ICP, CHN, BET, TEM, SEM, TPR and XRPD in order to verify loading of active metal present on the SiO_2 surface, to detect possible titanium contamination due to the use of a titanium-based US horn, to determine the presence of carbon in the samples, and to characterize the dispersion, nanostructure and size of the metal particles as well as morphological properties such as surface area, pore size and volume; with respect to traditional impregnated FT catalysts.

The samples were tested in a bench-scale FT rig with P = 2.0 MPa using a syngas with an H_2/CO molar ratio equal to 2. The experimental tests allowed the evaluation of catalytic activity in terms of CO conversion, selectivity towards various reaction products (*i.e.*, CH_4, CO_2, light and heavy hydrocarbons), stability over a prolonged time-on-stream (TOS) and a study of the composition of the heavy fraction over the various reaction temperatures ($T_{reac.}$ = 250, 255 and 260 °C) and activation temperatures ($T_{act.}$ = 350–400 °C) tested. Moreover, the experimental data collected allowed an evaluation of the effect of the iron and promoters loading on catalytic performance and the benefit of the sonochemical synthesis of FT catalysts with respect to the traditional impregnation method.

2. Experimental

In the present work, all the prepared catalysts are supported on SiO_2 and have been synthesized sonochemically, as described below. Sample composition is presented as weight percent and the samples are named Fe_{10}, Fe_{30} and $Fe_{30}K_2Cu_{3.75}$ where each subscript indicates weight percent of metal in the catalyst. When a comparison with traditional impregnated catalysts is made, they are labelled with the suffix IMP (impregnation). All the results in terms of CO conversion, selectivity towards the reaction products, carbon balance and C_{2+} yield are reported on a molar basis. Selectivity towards the products are divided into four categories: CO_2, CH_4, >C7 (heavy hydrocarbons with more than 7 carbon atoms) and <C7 (light hydrocarbons with less than 7 carbon atoms). The value of C_{2+} indicates the hydrocarbon yield without inclusion of undesired products such as CO_2 and CH_4 and is calculated using Eq. (6):

$$C_{2+}\ yield = \%CO_{Conversion} \cdot \frac{(>C7_{Selectivity} + <C7_{Selectivity})}{100} \quad (6)$$

2.1. Catalyst synthesis and characterization methods

2.1.1. Catalyst preparation

Sonochemical reactions were carried out in a round bottom glass reactor (V_{tot} = 15 mL); the distance from the US horn to the bottom of the reactor was 10 mm and was equipped with 3 different inlet/outlet glass pipes which allowed the measurement of the temperature (TC), the introduction of the reactants and the maintenance of an inert atmosphere (*i.e.*, argon). The US reactor and horn scheme is shown in Fig. 1.

The catalysts were prepared using a decomposition reaction of $Fe(CO)_5$ (Sigma-Aldrich) dissolved in *n*-decane (Sigma-Aldrich) in presence of dry silica (Fluka, BET s.a. = 515 $m^2 \cdot g^{-1}$) using US under argon flow; the support was dehydrated in air at 120 °C for 12 h. Before US exposure, SiO_2 and solvent were added to the ultrasonic reactor and all the atmospheric air was purged out using argon flow for 15 min. The presence of air inside the US reactor must be avoided in order to evade the contact of oxygen with the Fe^0 formed during the iron pentacarbonyl decomposition [11]. Once atmospheric air was eliminated from the reactor, $Fe(CO)_5$ was added. The US step was carried out over a 3 h duty cycle of 5/9 s at 20 kHz with an effective emitted power of 50 W. During the preparation of all three samples, the temperature inside the US reactor was kept lower than 25 °C over the duration of synthesis

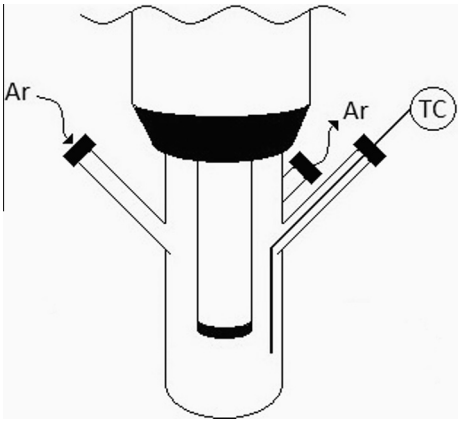

Fig. 1. Sonochemical reactor.

using a cooling bath. **Hazard note: very fine powders of metallic iron are pyrophoric and can be a safety hazard when exposed to air.**

The Fe_{10} samples were prepared using a precursor concentration of 0.08 M. The different loading of Fe was easily varied by changing the $Fe(CO)_5$ concentration in the *n*-decane solution. At the end of the US step, each catalyst was oxidized by flowing air over the *n*-decane solution for 18 h (air flux = 0.5 NL · h^{-1}) and then each solution was filtered and washed with pentane (Sigma-Aldrich).

The promoted potassium and copper containing catalysts were prepared using a previously optimized procedure in which an impregnation step on dry silica is added before sonochemical synthesis [20,21]. The wet impregnation of the precursors was carried out using an aqueous solution of 0.16 M KNO_3 (Sigma Aldrich) and 0.18 M $Cu(CH_3COO)_2$ (Sigma Aldrich) in a rotovap set to 26 rpm at 40 °C over 24 h. In an additional step, water was evaporated at 120 °C over 12 h and finally, calcined at 500 °C for 4 h.

2.1.2. Catalysts characterization

Characterization was carried out in part at the Frederick Seitz Materials Research Laboratory Central Research Facilities at University of Illinois. The elementary composition of each sample was measured with a PerkinElmer – SCIEX ELAN DRCe ICP-MS and a PerkinElmer 2400 Series II CHN/O Elemental Analyzer.

Catalyst surface area was determined by low temperature (−196 °C) N_2 adsorption using a Tristar II 3020 Micromeritics apparatus. Before measurement, samples were outgassed at 200 °C for 1 h under nitrogen flux. Surface area was calculated from nitrogen isotherms using BET theory from the instrumental software (Version 1.03).

The morphology of the samples was investigated using a JEOL 7000F analytical SEM and a JEOL 2100 Cryo TEM. X-ray powder diffraction (XRPD) patterns were taken with a SIEMENS/BRUKER D-5000 using CuKα emission, operating at 40 kV and 20 mA, with a step scan 0.5 °·min^{-1}, and in the 5–80 2θ range at room temperature (25 °C).

The Temperature Programmed Reduction analyses (TPR) were performed with a Thermoquest Mod. TPR/D/O 1100 equipped with a TCD detector. Samples were first pretreated with argon flow at 200 °C for 30 min, then a reducing mixture (5.1 vol% H_2 in Ar) was flowed in the samples (flux = 30 mL · min^{-1}) while increasing the temperature from 50 °C to 800 °C with a rate of 8 °C · min^{-1}.

2.2. Experimental bench scale tests

The experimental tests were carried out in a bench-scale fixed bed tubular reactor with an internal diameter of 6 mm and a length of the catalytic bed equal to 70 mm using 1 g of catalyst mixed with 1 g of α-Al_2O_3 (Fluka) which is catalytically inert and acts as diluent material in order to avoid the formation of local heating in the catalyst bed. The catalyst and diluent material were pressed into pellets and then crushed and sieved into aggregates with dimensions in the range 105–150 μm. Before experimental testing the catalysts were activated *in-situ* using a flow of syngas ($NL/h/g_{CAT}$ = 3.0) with a H_2/CO ratio equal to 2, at $T_{act.}$ = 350–400 °C and 0.4 MPa. The type of diluent, the mixture catalyst/Al_2O_3 ratio, and the activation procedure has been optimized in a previous work [22].

The catalytic activity was investigated at 250, 255 and 260 °C using a H_2/CO = 2 flow with $NL/h/g_{CAT}$ = 3.0 at 2.0 MPa. Before experimental testing, the syngas flow was mixed with 5.0 NmL · min^{-1} of an internal analytical standard (N_2).

The gas mixture after catalysis flow from the reactor, then passed into a cold trap (which operates at 5 °C and at the same pressure of the reactor); this trap allows the condensation of the water and heavy hydrocarbons produced. The >C7 fraction was analyzed by a gas chromatograph (Fisons-8000 series) equipped with a Porapack Q column (able to separate the C_7-C_{30} hydrocarbon fraction). The column temperature was maintained at 60 °C for 1 min and then raised to 300 °C at 8 °C · min^{-1}. The amount of carbonaceous species dissolved in water was determined with a total organic carbon analysis (TOC, Shimadzu 5000A).

Analysis of the light hydrocarbons and the unreacted gas not condensed in the cold trap was performed with an online micro-gas chromatograph (Agilent 3000A) every 120 min. This instrument is equipped with two different columns: (1) a molecular sieves module which can separate CO, N_2, and CH_4 at a column temperature of 100 °C, and (2) an OV-1 module (stationary phase of polydimethylsiloxilane) which can separate CO_2 and all hydrocarbons in the range C_2-C_6 at a column temperature of 45 °C.

Using all the collected data, the carbon molar balance resulted with a maximum error of ±5% moles for each run.

3. Results and discussion

3.1. Characterization results

Characterization of all catalyst samples was performed after sonochemical synthesis and before the reduction procedure. In some analyses, a comparison with traditional impregnated (IMP) catalysts is given (again performed before reduction). In addition, for TEM and SEM results, a comparison with the pristine commercial support (SiO_2) is also reported.

The effective amount of active metal and promoters, and the presence of titanium was determined in each sample by ICP analysis. The presence of carbon was determined by CHN analysis (Table 1). The results confirmed that the experimental amount of metals found in each samples is in good agreement with theoretical calculations; ICP results of impregnated samples are reported elsewhere [21]. The elementary analyses highlighted the presence of 0.009 ± 0.001 %wt of titanium and 1.5 ± 0.05 %wt of carbon. As reported in recent literature, the presence of a small amount of titanium does not affect FT catalysts performance [23] and carbon contamination does not constitute a problem since iron carbide is an active catalytic species for the FT synthesis [24]. The presence of titanium in the samples is due to SiO_2-Ti_{TIP} interaction during the US synthesis while the carbon is produced from the decomposition of alkane solvent or carbon monoxide during ultrasonic irradiation [8].

BET analyses indicated that the surface area of the catalyst decreased with increased loading of metals on the SiO_2 substrate; this result can be attributed to the diluting effect of the metals [20].

Table 1
Sample composition determined from ICP and BET results of sonochemical and impregnated samples.

Sample	Atom	Theoretical amount (%wt)	ICP results (%wt)	BET s.a. ($m^2 \cdot g^{-1}$)	Pore volume ($cm^3 \cdot g^{-1}$)	Pore diameter (nm)
Fe_{10} US	Fe	10	8.54	362	0.63	5.6
Fe_{30} US	Fe	30	29.66	314	0.54	5.7
$Fe_{30}K_2Cu_{3.75}$ US	Fe	30	29.86	216	0.50	6.8
	K	2	1.82			
	Cu	3.75	3.91			
Fe_{10} IMP				362		
Fe_{30} IMP				241		
$Fe_{30}K_2Cu_{3.75}$ IMP				133	0.33	7.2

Moreover, Fe_{10} US and Fe_{10} IMP had the same surface area while other samples synthesized (*i.e.*, Fe_{30} and $Fe_{30}K_2Cu_3$) with the use of US presented a bigger surface area in comparison to traditional impregnated samples on a SiO_2 support with the same metal loading. The benefits of the US preparation are more visible when a higher percentage of metals are supported on an inorganic support. Bulk metal (in this case, iron) has a very low surface area while the silica used as a support has a surface area equal to 515 $m^2 \cdot g^{-1}$. When inorganic supported materials, with low amount of metals (*e.g.* equal or lower than 10%) are synthesized, the BET results are not strongly influenced by the synthetic method used, since a low quantity of metal can be easily dispersed even with traditional techniques such as wetness impregnation. In Table 1 it is also evident that there is a decrease of the pore volume (about 0.1 $cm^3 \cdot g^{-1}$) with the increase of the metal loading while the pore diameter is not strongly influenced by the amount of the metals present.

The XRD diffractograms of all the samples, given in Fig. 2, do not reveal peaks related to iron oxides like Fe_2O_3 and Fe_3O_4 or iron-silicates. This finding is justified considering the formation of amorphous metal during the sonochemical synthesis of supported or bulk materials [8]. For SiO_2 supported iron-based catalysts, the transition from amorphous solid to crystalline structure is usually obtained with a thermal treatment at 350 °C over 6 h [11] but even if all the reported samples are oxidized from air present after the sonochemical synthesis, temperatures equal to or higher than 350 °C were not reached.

The TPR profiles of all the sonochemically synthesized samples with a comparison to traditionally impregnated iron-based catalysts are given in Fig. 3. For all iron catalysts, two different reduction steps are present; the first one is attributable to the transition from hematite (Fe_2O_3) to magnetite (Fe_3O_4) which is one of the active species for the FT process at 250–350 °C while the last one is due to the reduction from magnetite to α-Fe at 450–750 °C. The first peak (associated with the first reduction step) in the TPR profile for the Fe_{10} and Fe_{30} samples, using both US and IMP, was present at the same reduction temperature (350 °C). The effect of copper addition is also shown in the TPR profiles of the promoted samples ($Fe_{30}K_2Cu_{3.75}$ and $Fe_{30}K_2Cu_{3.75}$ IMP) and, in comparison to the un-promoted samples, they present a left shift to lower reduction temperatures for both reduction steps; an indication of better the mixing of the metals and increased activity of the promoter. A possible mechanism for the promotion effect involves the migration of hydrogen atoms from reduced Cu to the iron oxides [25]. $Fe_{30}K_2Cu_{3.75}$ IMP yields lower reduction temperatures with respect to all the other catalysts; possibly due to the fact that this is the only sample in which iron and copper are added at the same time during the wet impregnation step thus a better contact between iron oxide and copper oxide particles on the SiO_2 surface can be achieved.

TEM and SEM images are shown in Fig. 4. They highlight that samples synthesized with the use of US present uniform and well dispersed iron nanoparticles; a comparison with the un-loaded SiO_2 support is also given. TEM images show that the Fe nanoparticles (black areas) have dimensions less than 20 nm and no larger aggregates were found in any of the catalysts.

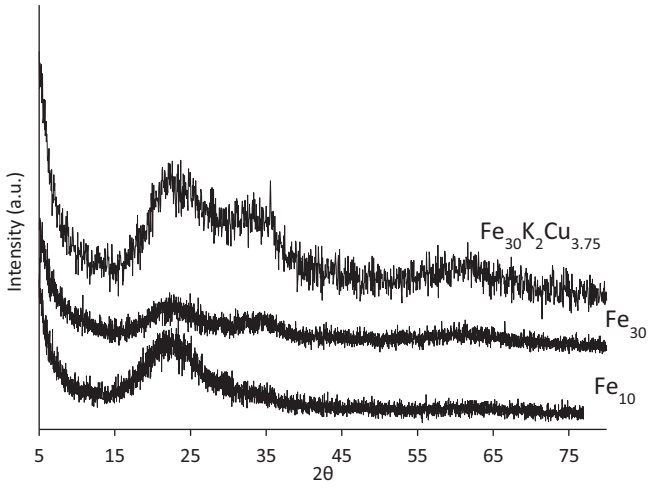

Fig. 2. XRPD of Fe_{10}, Fe_{30} and $Fe_{30}K_2Cu_{3.75}$.

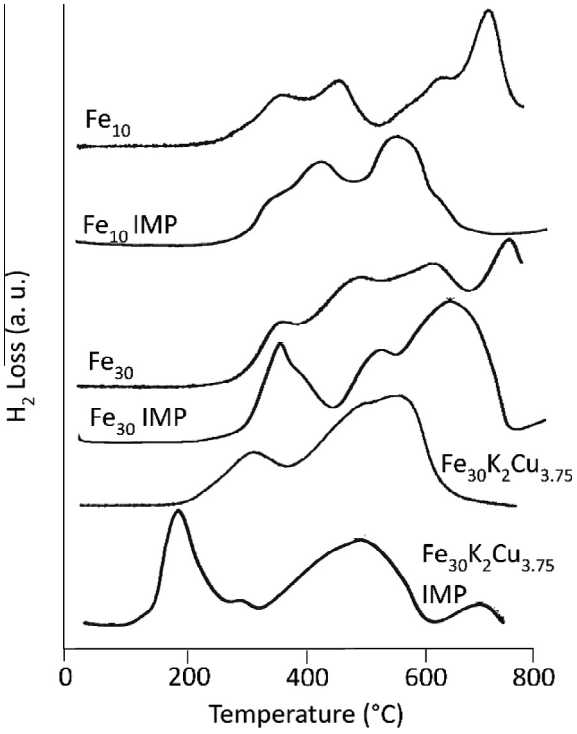

Fig. 3. Comparison among the TPR profiles of Fe_{10}, Fe_{30}, $Fe_{30}K_2Cu_{3.75}$, Fe_{10} IMP, Fe_{30} IMP and $Fe_{30}K_2Cu_{3.75}$ IMP.

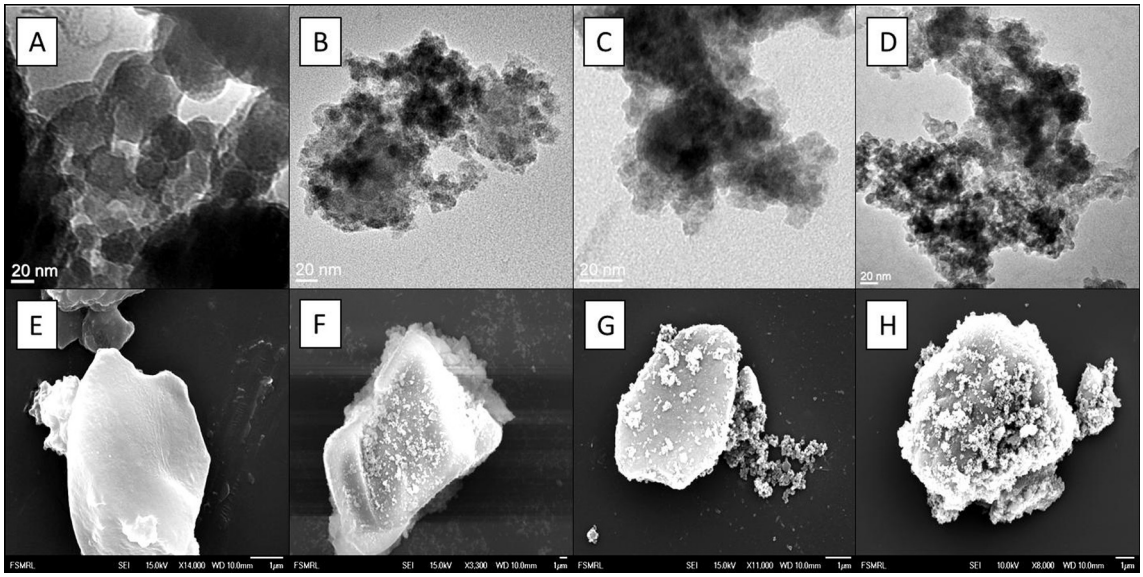

Fig. 4. TEM and SEM images of: SiO_2 (A, E); Fe_{10} (B, F); Fe_{30} (C, G); $Fe_{30}K_2Cu_{3.75}$ (D, H).

SEM images show that the surface of the support without Fe is very smooth (Fig. 4-E) while, with an increase in the metal loading, Fe agglomerates begin to form on the SiO_2 surface. In the case of $Fe_{30}K_2Cu_{3,75}$ the active metal and promoter agglomerates are better dispersed.

3.2. Fischer-Tropsch catalytic tests

The experimental data obtained during testing in the FT bench-scale rig have been measured from the beginning of the test until the process reached the steady state. The experimental results are reported in terms of rate of CO conversion, selectivity (%) towards CO_2 and CH_4 (undesired by-products of the process), light hydrocarbons (<C7 fraction), heavy hydrocarbons (>C7 fraction) and total yield of C_{2+}. Moreover, analysis of the heavy organic fraction collected in the cold trap was done in three different groups (C_{7-9}, C_{10-15}, and C_{16-30}).

The results of the samples reported in Fig. 5 and Table 2 allow the evaluation of catalyst stability in terms of rate of CO conversion as a function of TOS and reaction temperature, the difference in selectivity towards the reaction products and the yield of C_{2+}. In particular, the rate of CO conversion is slightly influenced by the activation temperature for the Fe_{10} sample. In fact, an increase of

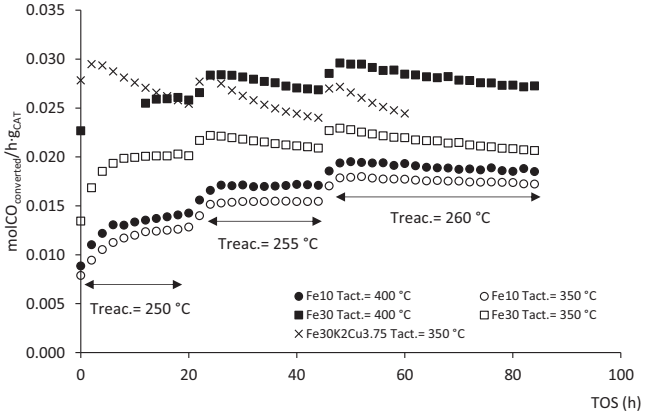

Fig. 5. Rate of CO conversion as a function of TOS and activation temperature for the Fe_{10}, Fe_{30} and $Fe_{30}K_2Cu_{3.75}$ samples.

Table 2
C_{2+} yield and product selectivity of sonochemical catalysts.

Sample	$T_{act.}$ (°C)	$T_{reac.}$ (°C)	$molCO_{converted}/h \cdot g_{CAT}$	C_{2+} yield	Selectivity (%)			
					CH_4	CO_2	<C_7	>C_7
Fe_{10}	400	250	0.014	30.2	5	5	18	72
		255	0.017	36.4	5	6	18	71
		260	0.018	39	5	7	18	70
	350	250	0.013	27.6	5	5	19	71
		255	0.015	32.9	5	6	19	70
		260	0.017	36.3	5	7	19	69
Fe_{30}	400	250	0.026	54.3	4	9	17	70
		255	0.027	54	4	12	18	66
		260	0.028	54.8	4	12	17	67
	350	250	0.020	42.8	4	7	19	71
		255	0.021	44.0	4	8	19	70
		260	0.021	43.0	4	9	19	69
$Fe_{30}K_2Cu_{3.75}$	350	250	0.025	48.1	3	18	14	65
		255	0.024	45.3	3	18	14	65
		260	0.024	45.1	3	20	14	63

≈0.001 $molCO_{converted}/h \cdot g_{CAT}$ was detected with increasing activation temperature (T_{act}) from 350 °C to 400 °C, for all reaction temperatures (T_{reac}) tested. However, the effect of activation temperature is more pronounced for the Fe_{30} sample where the increase in the rate of moles of CO converted is equal to 0.004 $molCO_{converted}/h \cdot g_{CAT}$ at $T_{reac.}$ = 250 °C and almost 0.007 $molCO_{converted}/h \cdot g_{CAT}$ at $T_{reac.}$ = 255–260 °C by raising the reduction temperature to $T_{act.}$ = 400 °C. Moreover, both Fe_{10} and Fe_{30} catalysts show a satisfactory stability as a function of TOS at all temperature tested. $Fe_{30}K_2Cu_{3.75}$ did not show any catalytic activity if reduced to $T_{act.}$ = 400 °C, due to the high activity of this sample towards the Boudouard reaction which rapidly produces elementary carbon on the catalyst surface thus resulting in a complete deactivation of the sample. The formation of this elementary carbon blocks iron carbide activity for FTS [26] and, even though the activation was carried out at $T_{act.}$ = 350 °C, the promoted sample showed a great decrease in catalytic activity as a function of TOS at the three tested reaction temperatures.

Selectivity towards the reaction products is not significantly influenced by the reaction temperature in the range 250–260 °C and the selectivity value towards CH_4 is low (≈4%) for all the catalysts under the tested experimental condition. The Fe_{10} sample

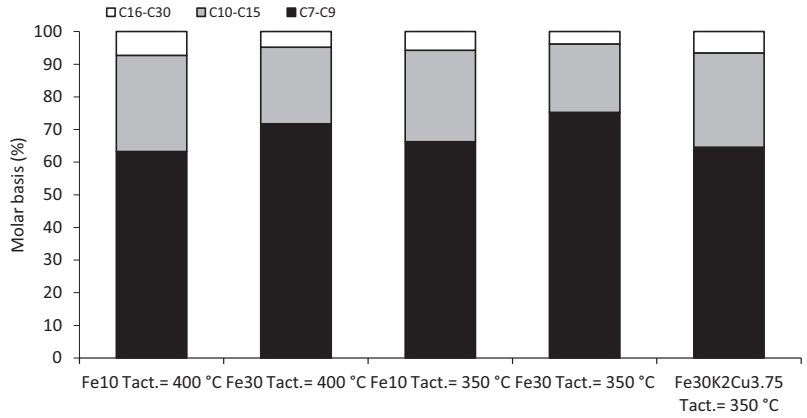

Fig. 6. Composition of the heavy organic phase (>C7) for US samples activated at $T_{act.}$ = 350–400 °C and tested at $T_{reac.}$ = 255 °C.

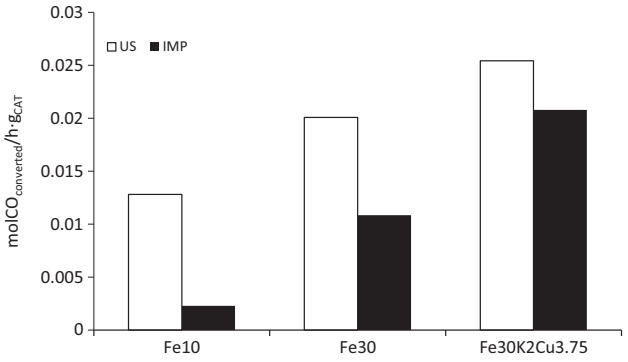

Fig. 7. Comparison between US and IMP samples in terms of rates of CO conversion at $T_{reac.}$ = 250 °C.

presents the best selectivity for the heavy hydrocarbon fraction (72%) when tested with $T_{act.}$ = 400 °C and a reaction temperature of 250 °C. The promoted samples show greater selectivity for CO_2 (20%) with respect to the other US synthesized catalysts. The Fe_{10} sample showed little change in selectivity as a function of the activation temperatures tested. However, a slight increase in selectivity towards CO_2 from 8% to 12% was observed for the Fe_{30} sample from $T_{act.}$ = 350 °C to $T_{act.}$ = 400 °C.

The results from the GC analysis performed on the heavy organic fraction collected in the cold trap during tests performed at $T_{reac.}$ = 255 °C and various activation temperatures are shown in Fig. 6. The molar composition of the heavy fraction C_7-C_{30} is not strongly influenced by activation temperature; moreover Fe_{10} activated at both temperatures and $Fe_{30}K_2Cu_{3.75}$ yielded almost the same molar fraction for the three groups ($C_{7\text{-}9}$, $C_{10\text{-}15}$, $C_{16\text{-}30}$) with only the Fe_{30} sample showing a slight increase in the $C_{7\text{-}9}$ fraction at both temperatures with respect to the other samples. The composition of the >C7 phase for all samples presented is in agreement with other reports [27,28].

A comparison between catalytic performance by the sonochemical samples versus traditional impregnated catalysts is shown in Figs. 7 and 8. Catalytic activity, at $T_{reac.}$ = 250 °C, was higher in sonochemically prepared catalysts over IMP samples with the same amount of active metal and promoters; in particular an increase of about 5 times was observed for the Fe_{10} sample. All the US samples had lower selectivity to methane, in particular Fe_{10} methane selectivity is 6 times lower while Fe_{30} and $Fe_{30}K_2Cu_{3.75}$ methane selectivity decreased bout 50% with respect to IMP samples. The measured selectivity to CO_2 is lower for US Fe_{10} and Fe_{30} while $Fe_{30}K_2Cu_{3.75}$ presented the highest selectivity value towards carbon dioxide. All the US synthesized catalysts showed higher selectivity to >C7 with respect to the IMP samples.

The improved reactant conversion and selectivity values using the US samples can be attributed to the production of nanostructured materials with better surface and morphological properties; a benefit of US synthesis. In particular, US synthesized samples presented smaller iron nanoparticles (20 nm) than the traditional IMP samples (>50–60 nm), resulting in greater catalytic activity [29]. The US catalysts showed a larger pore volume than IMP samples, which allows for higher iron loading without blocking pores. This large pore volume may also help in uniform distribution of the active phase into the pore and greater accessibility of the active phase to the reactants [30].

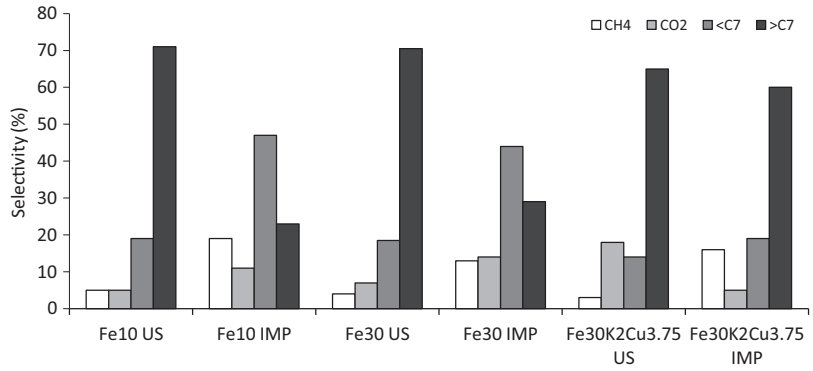

Fig. 8. Comparison between US and IMP samples in terms of product selectivity at $T_{reac.}$ = 250 °C.

4. Conclusion

Three different iron-based SiO_2 supported FT catalysts with various loadings of active metal and promoters have been synthesized with the use of ultrasound.

Surface analyses showed that Fe_{30} and $Fe_{30}K_2Cu_{3.75}$ synthesized with US presented a larger surface area when compared with traditional impregnated catalysts. The active metal nanoparticles are well dispersed on the surface of the oxide support and have dimensions of about 20 nm. TPR profiles showed that both Fe_{10} and Fe_{30} samples presented the same reduction temperature ($T_{act.}$ = 350 °C) while potassium and copper promotion shifted the first reduction peak about 50 °C to lower temperatures.

From experimental testing under catalytic conditions, all the US synthesized samples are suitable catalysts for the FT reaction under various testing conditions and with an H_2/CO ratio equal to 2. Both Fe_{10} and Fe_{30} catalysts showed excellent stability as a function of TOS under all tested reaction temperatures. An increase in activation temperature from 350 °C to 400 °C results in an increase in rate of CO conversion whereas selectivity towards the reaction products is not largely influenced by activation or reaction temperature.

The sonochemically prepared catalysts showed good results in terms of selectivity towards C_{2+} hydrocarbons fraction and methane with average values of S_{CH4} = 4%, $S_{<C7}$ = 16%, $S_{>C7}$ = 70%; moreover, the molar composition of the heavy fraction (C_7-C_{30}) is not strongly influenced by activation temperature.

Ultrasound synthesized catalysts provided higher steady state rates of CO conversion and better selectivity towards reaction products when compared to traditional impregnated catalysts.

Acknowledgments

The authors gratefully acknowledge Maria LaGasse for the text review.

References

[1] J.H. Bang, K.S. Suslick, Applications of ultrasound to the synthesis of nanostructured materials, Adv. Mater. 22 (2010) 1039–1059, http://dx.doi.org/10.1002/adma.200904093.
[2] H. Xu, B.W. Zeiger, K.S. Suslick, Sonochemical synthesis of nanomaterials, Chem. Soc. Rev. 42 (2013) 2555–2567, http://dx.doi.org/10.1039/c2cs35282f.
[3] D.G. Shchukin, E. Skorb, V. Belova, H. Möhwald, Ultrasonic cavitation at solid surfaces, Adv. Mater. 23 (2011) 1922–1934, http://dx.doi.org/10.1002/adma.201004494.
[4] J.P. Wilcoxon, B.L. Abrams, Synthesis, structure and properties of metal nanoclusters, Chem. Soc. Rev. 35 (2006) 1162–1194, http://dx.doi.org/10.1039/b517312b.
[5] S. Anandan, M. Ashokkumar, Sonochemical Synthesis of Noble Monometallic and Bimetallic Nanoparticles for Catalytic Applications, 2014, http://dx.doi.org/10.1201/b15669-4.
[6] K. Suslick, S. Skrabalak, Sonocatalysis, Handb. Heterog. Catal. 4 (2008) 2007–2017.
[7] K.S. Suslick, D.J. Flannigan, Inside a collapsing bubble: sonoluminescence and the conditions during cavitation, Annu. Rev. Phys. Chem. 59 (2008) 659–683, http://dx.doi.org/10.1146/annurev.physchem.59.032607.093739.
[8] K.S. Suslick, T. Hyeon, M. Fang, A.A. Cichowlas, Sonochemical synthesis of nanostructured catalysts, Mater. Sci. Eng., A 204 (1995) 186–192.
[9] A. Di Michele, P. Sassi, A. Comazzi, F. Galli, C. Pirola, C.L. Bianchi, Co- and Co (Ru)-based catalysts for Fischer-Tropsch synthesis prepared by high power ultrasound, Mater. Focus. 4 (2015) 295–301, http://dx.doi.org/10.1166/mat.2015.1273.
[10] C. Pirola, C.L. Bianchi, A. Di Michele, P. Diodati, D. Boffito, V. Ragaini, Ultrasound and microwave assisted synthesis of high loading Fe-supported Fischer-Tropsch catalysts, Ultrason. Sonochem. 17 (2010) 610–616, http://dx.doi.org/10.1016/j.ultsonch.2009.11.004.
[11] K.S. Suslick, T. Hyeon, M. Fang, Nanostructured materials generated by high-intensity ultrasound: sonochemical synthesis and catalytic studies, Chem. Mater. 8 (1996) 2172–2179, http://dx.doi.org/10.1021/cm960056l.
[12] W. Ma, G. Jacobs, D.E. Sparks, J.L.S. Klettlinger, C.H. Yen, B.H. Davis, Fischer-Tropsch synthesis and water gas shift kinetics for a precipitated iron catalyst, Catal. Today (2016), http://dx.doi.org/10.1016/j.cattod.2016.01.006.
[13] B. Todic, L. Nowicki, N. Nikacevic, D.B. Bukur, Fischer-Tropsch synthesis product selectivity over an industrial iron-based catalyst: effect of process conditions, Catal. Today 261 (2016) 28–39, http://dx.doi.org/10.1016/j.cattod.2015.09.005.
[14] P.K. Swain, L.M. Das, S.N. Naik, Biomass to liquid: a prospective challenge to research and development in 21st century, Renew. Sustain. Energy Rev. 15 (2011) 4917–4933, http://dx.doi.org/10.1016/j.rser.2011.07.061.
[15] S.S. Ail, S. Dasappa, Biomass to liquid transportation fuel via Fischer Tropsch synthesis – technology review and current scenario, Renew. Sustain. Energy Rev. 58 (2016) 267–286, http://dx.doi.org/10.1016/j.rser.2015.12.143.
[16] C. Pirola, A. Di Fronzo, F. Galli, C.L. Bianchi, A. Comazzi, F. Manenti, Biosyngas conversion by Fischer-Tropsch synthesis: experimental results and multi-scale simulation of a PBR with high Fe loaded supported catalysts, Chem. Eng. Trans. 37 (2014) 595–600.
[17] C. Pirola, C.L. Bianchi, A. Di Michele, S. Vitali, V. Ragaini, Fischer Tropsch and Water Gas Shift chemical regimes on supported iron-based catalysts at high metal loading, Catal. Commun. 10 (2009) 823–827, http://dx.doi.org/10.1016/j.catcom.2008.12.006.
[18] G.P. Van Der Laan, A.A.C.M. Beenackers, Kinetics and selectivity of the Fischer-Tropsch synthesis: a literature review, Catal. Rev. Sci. Eng. 41 (1999) 255–318, http://dx.doi.org/10.1016/j.apcata.2013.10.061.
[19] A.N. Pour, M.R. Housaindokht, S.F. Tayyari, J. Zarkesh, Kinetics of the water-gas shift reaction in Fischer-Tropsch synthesis over a nano-structured iron catalyst, J. Nat. Gas Chem. 19 (2010) 362–368, http://dx.doi.org/10.1016/S1003-9953(09)60085-2.
[20] A. Comazzi, C. Pirola, C.L. Bianchi, F. Galli, M. Longhi, F. Manenti, High-loaded Fe-supported catalyst for the thermochemical BTL-FT process: experimental results and modelling, Can. J. Chem. Eng. 9999 (2015) 1–7, http://dx.doi.org/10.1002/cjce.22357.
[21] C. Pirola, L. Bianchi, A. Di Michele, P. Diodati, S. Vitali, V. Ragaini, High loading Fe-supported fischer-Tropsch catalysts: optimization of the catalyst performance, Catal. Lett. 131 (2009) 294–304. doi:10.1007/s10562-009-0060-6.
[22] A. Di Fronzo, C. Pirola, A. Comazzi, F. Galli, C.L. Bianchi, A. Di Michele, et al., Co-based hydrotalcites as new catalysts for the Fischer-Tropsch synthesis process, Fuel 119 (2014) 62–69, http://dx.doi.org/10.1016/j.fuel.2013.11.014.
[23] K. Shimura, T. Miyazawa, T. Hanaoka, S. Hirata, Fischer-Tropsch synthesis over alumina supported cobalt catalyst: effect of promoter addition, Appl. Catal. A Gen. 494 (2015) 1–11, http://dx.doi.org/10.1016/j.apcata.2015.01.017.
[24] M.K. Gnanamani, G. Jacobs, U.M. Graham, M.C. Ribeiro, F.B. Noronha, W.D. Shafer, et al., Influence of carbide formation on oxygenates selectivity during Fischer-Tropsch synthesis over Ce-containing Co catalysts, Catal. Today 261 (2016) 40–47, http://dx.doi.org/10.1016/j.cattod.2015.08.047.
[25] Y. Jin, A.K. Datye, Phase transformations in iron Fischer-Tropsch catalysts during temperature-programmed reduction, J. Catal. 196 (2000) 8–17, http://dx.doi.org/10.1006/jcat.2000.3024.
[26] S. Li, S. Krishnamoorthy, A. Li, G.D. Meitzner, E. Iglesia, Promoted iron-based catalysts for the Fischer-Tropsch synthesis: design, synthesis, site densities, and catalytic properties, J. Catal. 206 (2002) 202–217, http://dx.doi.org/10.1006/jcat.2001.3506.
[27] S. Abelló, D. Montané, Exploring iron-based multifunctional catalysts for Fischer-Tropsch synthesis: a review, ChemSusChem 4 (2011) 1538–1556, http://dx.doi.org/10.1002/cssc.201100189.
[28] Y. Zamani, Fischer-Tropsch synthesis over nano-sized iron-based catalysts: investigation of promoter and temperature effects on products distribution, Pet. Coal 57 (2015) 71–75.
[29] K. Cheng, V.V. Ordomsky, M. Virginie, B. Legras, P.A. Chernavskii, V.O. Kazak, et al., Support effects in high temperature Fischer-Tropsch synthesis on iron catalysts, Appl. Catal. A Gen. 488 (2014) 66–77, http://dx.doi.org/10.1016/j.apcata.2014.09.033.
[30] K. Keyvanloo, W.C. Hecker, B.F. Woodfield, C.H. Bartholomew, Highly active and stable supported iron Fischer-Tropsch catalysts: effects of support properties and SiO_2 stabilizer on catalyst performance, J. Catal. 319 (2014) 220–231, http://dx.doi.org/10.1016/j.jcat.2014.08.015.